ARMY RESEARCH LABORATORY

The Pyramid Liner Concept

by William P. Walters and Daniel R. Scheffler

ARL-TR-2995 **June 2003**

NOTICES

Disclaimers

The findings in this report are not to be construed as an official Department of the Army position unless so designated by other authorized documents.

Citation of manufacturer's or trade names does not constitute an official endorsement or approval of the use thereof.

Destroy this report when it is no longer needed. Do not return it to the originator.

Army Research Laboratory
Aberdeen Proving Ground, MD 21005-5066

ARL-TR-2995 **June 2003**

The Pyramid Liner Concept

William P. Walters and Daniel R. Scheffler
Weapons and Materials Research Directorate, ARL

Report Documentation Page

Form Approved
OMB No. 0704-0188

1. REPORT DATE *(DD-MM-YYYY)*	2. REPORT TYPE	3. DATES COVERED (From - To)
June 2003	Final	September 2001–September 2002

4. TITLE AND SUBTITLE
The Pyramid Liner Concept

5a. CONTRACT NUMBER

5b. GRANT NUMBER

5c. PROGRAM ELEMENT NUMBER

6. AUTHOR(S)
William P. Walters and Daniel R. Scheffler

5d. PROJECT NUMBER
1L162618AH80

5e. TASK NUMBER

5f. WORK UNIT NUMBER

7. PERFORMING ORGANIZATION NAME(S) AND ADDRESS(ES)
U.S. Army Research Laboratory
ATTN: AMSRL-WM-TC
Aberdeen Proving Ground, MD 21005-5066

8. PERFORMING ORGANIZATION REPORT NUMBER
ARL-TR-2995

9. SPONSORING/MONITORING AGENCY NAME(S) AND ADDRESS(ES)

10. SPONSOR/MONITOR'S ACRONYM(S)

11. SPONSOR/MONITOR'S REPORT NUMBER(S)

12. DISTRIBUTION/AVAILABILITY STATEMENT
Approved for public release; distribution is unlimited.

13. SUPPLEMENTARY NOTES

14. ABSTRACT

A shaped charge device was designed from a charge with a four-sided pyramid as the liner. Devices of this nature were first studied by Geiger and Honcia in 1977 and relegated to the area of interesting concepts, but without application. The current study represents probably the first numerical simulations of this charge, including parametric variations of the altitude of the pyramid and the initiation mode of the explosive. The numerical simulations were performed using the CTH hydrocode (shock physics code) developed by Sandia National Laboratories. The liner was made of copper, and the wall thickness of each isosceles triangle comprising the pyramid was identical. The multiple interacting jets provide a wide area of coverage that implies that the device may be useful as a multidirectional cutting charge. A multidirectional charge may be useful for certain applications in the mining, oil well completion, demolition, or military fields.

15. SUBJECT TERMS
shaped charge, pyramid liners, jet growth, jet formation, simulation, hydrocode

16. SECURITY CLASSIFICATION OF:			17. LIMITATION OF ABSTRACT	18. NUMBER OF PAGES	19a. NAME OF RESPONSIBLE PERSON
a. REPORT	b. ABSTRACT	c. THIS PAGE			William P. Walters
UNCLASSIFIED	UNCLASSIFIED	UNCLASSIFIED	UL	34	19b. TELEPHONE NUMBER (*Include area code*) 410-278-6062

Standard Form 298 (Rev. 8/98)
Prescribed by ANSI Std. Z39.18

Contents

List of Figures

List of Tables

1. Introduction

A numerical study was performed on shaped charges that employed a pyramid as the liner geometry. The CTH hydrocode (McGlaun et al., 1990) developed by Sandia National Laboratories was used in this study. The pyramid had a square base with the diagonal of the base equal to 1.4 cm. The altitude (or height) of the pyramid was varied from 0.5 to 1.31 cm. The thickness of each face of the pyramid was 0.06 cm, and the liner material was copper. The explosive geometry was a right circular cylinder with a diameter of 1.4 cm and a height of 2.31 cm. The charge was bare (i.e., uncased), and cyclotetramethylenetetranitramine (HMX) was used as the explosive fill. Also, a square-shaped explosive fill was studied with a base diagonal of 1.4 cm and a height of 2.31 cm enclosing the 1.31-cm altitude pyramid. The initiation mode was varied for this explosive geometry, including a single-point detonation, a line wave detonation, a four-point detonation, and a five-point detonation.

Geiger and Honcia (1977) conducted earlier studies with square-based pyramidal liners. They presented flash radiographs of six pyramidal liner shapes each with the same base area, the base diagonal being 4.0 cm. The current study is a numerical investigation of square-based pyramidal liners using the January 2002 version of the CTH hydrocode (McGlaun et al., 1990), which is a state-of-the-art, second-order accurate, Eulerian hydrocode under continuous development at Sandia National Laboratories, NM. CTH is capable of solving complex problems in shock physics in one, two, or three dimensions. Previous studies have verified that CTH hydrocode simulations are generally in excellent agreement with experimental data. The code provides several constitutive models, including an elastic-perfectly plastic model with provisions for work hardening and thermal softening, the Johnson-Cook model (Johnson and Cook, 1983), the Zerilli-Armstrong model (Zerilli and Armstrong, 1987), the Steinberg-Guinan-Lund model (Steinberg et al., 1980; Steinberg and Lund, 1989), an undocumented power-law model, and others. Detonation of the high explosive (HE) can be modeled using the programmed burn model, the Chapman-Jouguet volume burn models, or the history variable reactive burn model (Kerley, 1992). Several equation of state (EOS) options are available, including tabular (i.e., SESAME), analytical (ANEOS), Mie-Grüneisen, and Jones-Wilkins-Lee (JWL) (Lee et al., 1968). Material failure occurs when a threshold value of tensile stress or hydrostatic pressure is exceeded. In addition, the Johnson-Cook failure model (Johnson and Cook, 1985) is also available. When failure occurs in a cell, void is introduced until the stress state of the cell is reduced to zero. Recompression is permitted. To reduce the diffusion typically encountered in Eulerian simulations, several advanced material interface tracking algorithms are provided, including the high-resolution interface tracking (HRIT) algorithm (available for two-dimensional [2-D] simulations only), the simple line interface calculation (SLIC) algorithm (Noh and Woodward, 1976), and the Sandia-modified Young's reconstruction algorithm (SMYRA) (Bell and Hertel, 1992). The following sections describe the CTH code input, present the numerical results, and discuss these results.

2. Problem Setup

All simulations were performed in quarter symmetry with the origin of the coordinate system located in the center of the square base of the pyramid and the main jet formation and movement along the +y coordinate direction. The planes of symmetry were located at x = 0 and z = 0. For each of the simulations, the mesh consisted of 130 × 750 × 130 cells with each cell having dimensions of 0.01 × 0.01 × 0.01 cm. The mesh in the y coordinate direction started at −2.5 cm and ended at 5.0 cm. In order to capture the main jet's velocity history, a Lagrangian tracer particle was inserted into the mesh at the <0, −0.02, 0> cm coordinate position.

The copper liners were modeled using standard copper properties for the Johnson-Cook constitutive model (Johnson et al., 1983) and CTH library values for the Mie-Grüneisen EOS. Failure was modeled using a simple tensile pressure criteria such that failure would occur at a tensile pressure of 345.0 MPa. The HMX explosive was treated as a fluid (i.e., it does not support strength). The JWL EOS was used to model the pressure-volume-energy behavior of the detonation products of the HMX explosive using parameters from Dobratz (1981). A simple programmed burn model was used to model explosive initiation.

An input deck used for the liner height study is given in Appendix A for the case of the 0.5-cm liner. Comments included in the input deck give the changes needed to modify the CTH input for the other liner geometries. Appendix B includes the input deck for the detonation initiation study for the one-point initiation case. Comments included in the input deck give the modifications needed for the other included initiation modes.

3. Numerical Results and Discussion

The altitude of the pyramidal liner was varied from 0.5 to 1.31 cm with corresponding pyramid angles (i.e., the angle between opposing faces of the pyramid), varying from 89.4° to 41.4°. The geometry and mass of the explosive and liner for each case are given in Table 1. Figure 1 depicts the initial geometry. Figures 2–6 present the results of the simulations. Each figure represents a different time but the same distance of travel. Each comparison was made before the jet tip had traveled ~5 cm (just before it left the computational mesh). Each figure shows a side view (from the +z direction), a top view (from the +y direction), and a rotated view (rotated 45° about the y-axis then rotated 45° toward the reader to illustrate the three-dimensional [3-D] nature of the jet). While the simulations were performed in quarter symmetry, the geometry was reflected in such a way as to show the whole jet. In all figures, the side views are to the same scale. The top views are also to the same scale in all figures but not to the same scale as the side views. Likewise, the rotated views scale for all figures but not to the side or top views. Figure 2

Table 1. Geometry and mass of the pyramidal liners and cylindrical explosive billets.

Pyramid Altitude (cm)	HE Height (cm)	Pyramid Wall Thickness (cm)	Pyramid Base Diagonal (cm)	Pyramid Angle (°)	Pyramid Mass (g)	Charge Mass (g)
0.50	2.31	0.06	1.40	89.4212	0.15881	1.60387
0.70	2.31	0.06	1.40	70.5288	0.19531	1.57298
0.92	2.31	0.06	1.40	56.5619	0.24082	1.53900
1.00	2.31	0.06	1.40	52.6685	0.25786	1.52665
1.31	2.31	0.06	1.40	41.3975	0.32557	1.47877

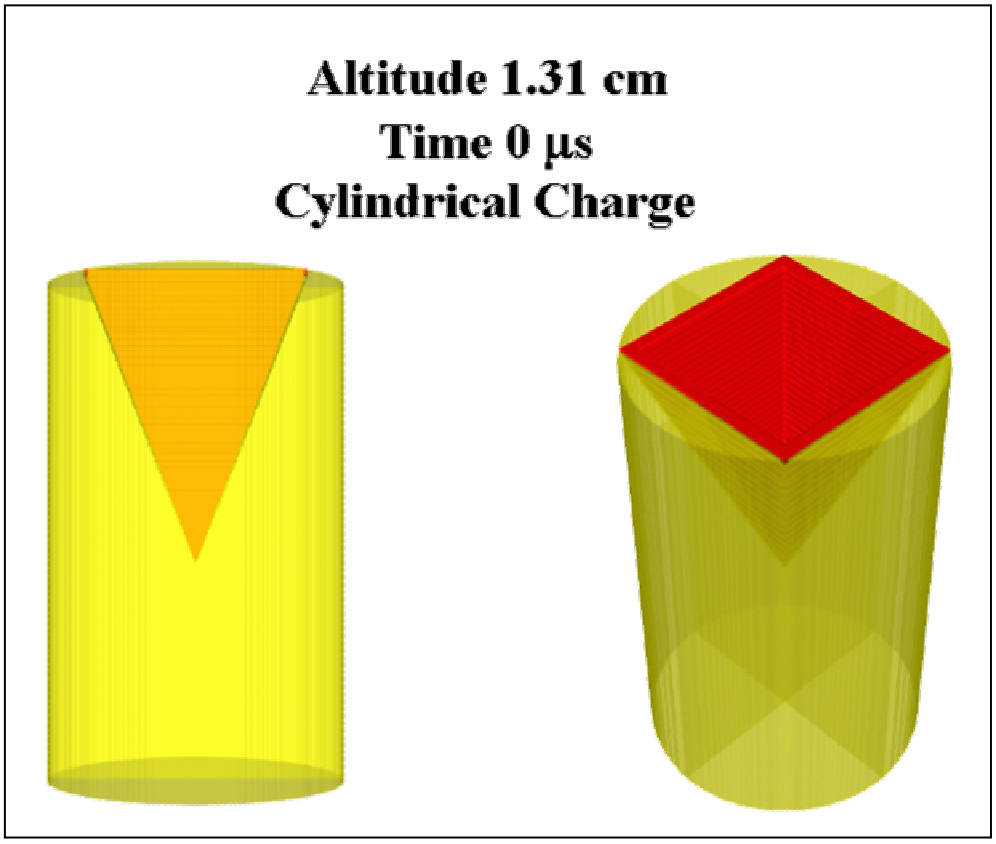

Figure 1. Initial geometry of the 1.31-cm altitude pyramidal liner with a cylindrical explosive billet.

shows the jet from the pyramidal liner with an altitude of 0.5 cm at 12 μs. The jet tip velocity (i.e., the maximum velocity along the jet centerline) was 5.1 km/s. Probes were also used in conjunction with the code to estimate velocities near the tip region and on the trailing wings. These probes are shown as violet dots in these regions and their position is somewhat arbitrary. Figure 2's side view shows a 2-D projection on the x-y plane as viewed from the +z axis of the jet formation and growth. Figure 2's top view shows the top view, again with the probe locations, and Figure 2's rotated view is the rotated view again with the probe locations shown.

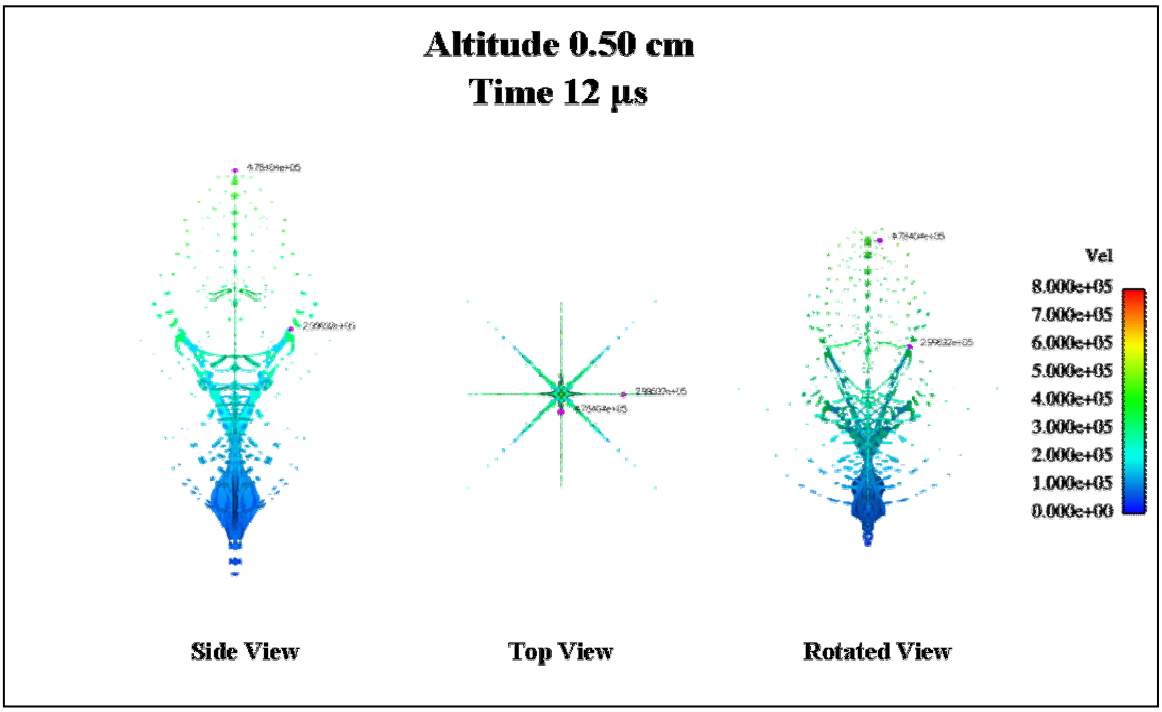

Figure 2. Formation of the 0.50-cm altitude pyramid charge at 12 µs.

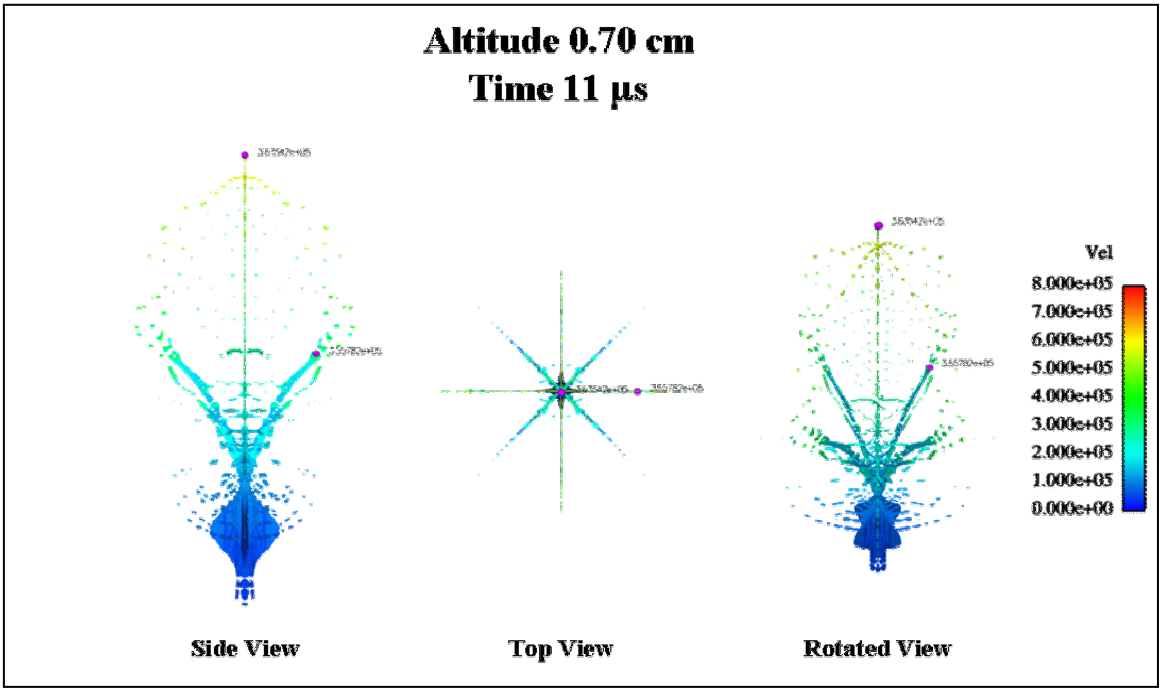

Figure 3. Formation of the 0.70-cm altitude pyramid charge at 11 µs.

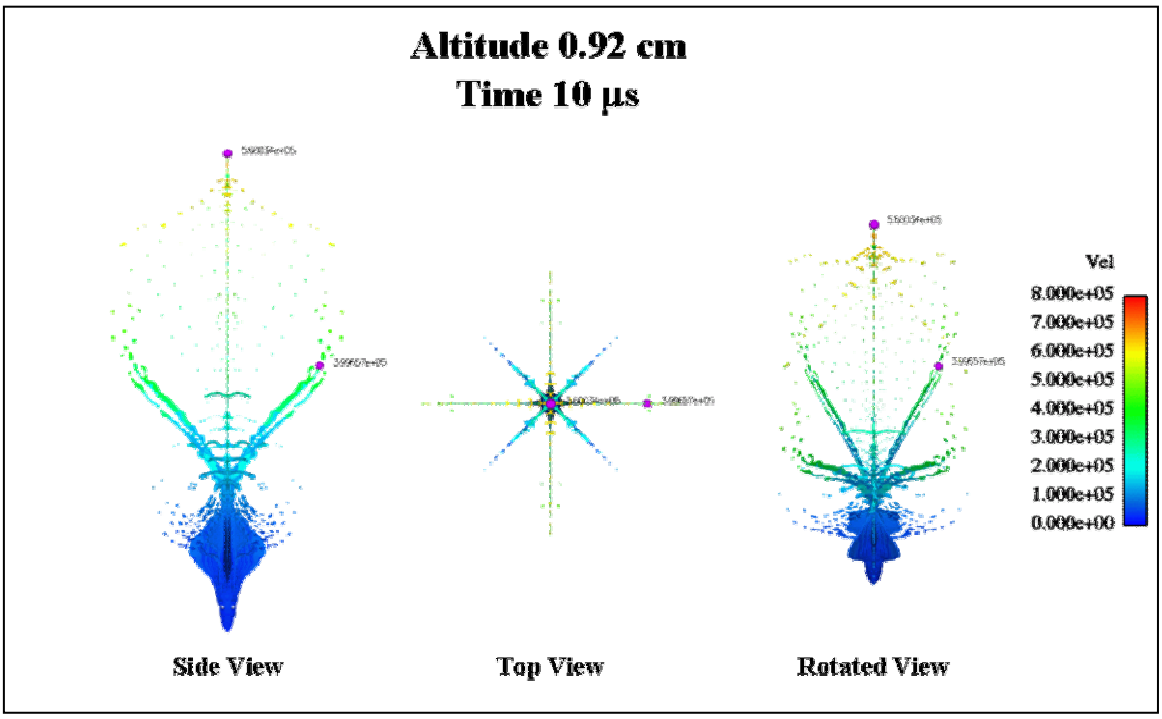

Figure 4. Formation of the 0.92-cm altitude pyramid charge at 10 µs.

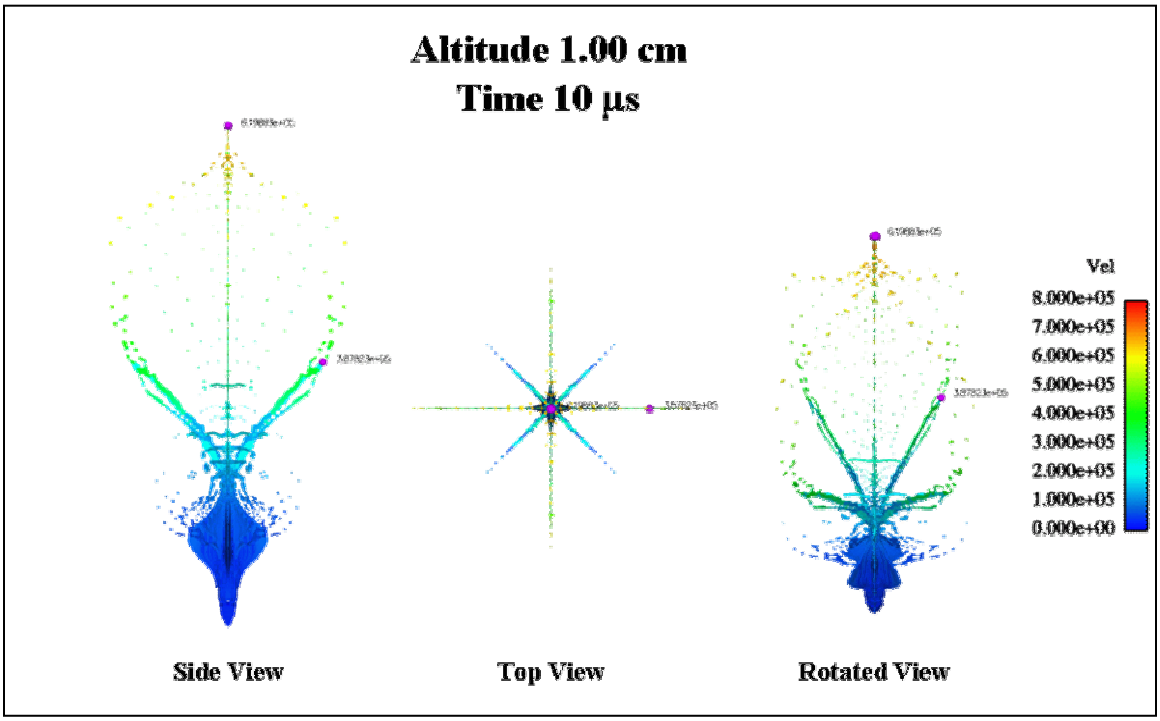

Figure 5. Formation of the 1.00-cm altitude pyramid charge at 10 µs.

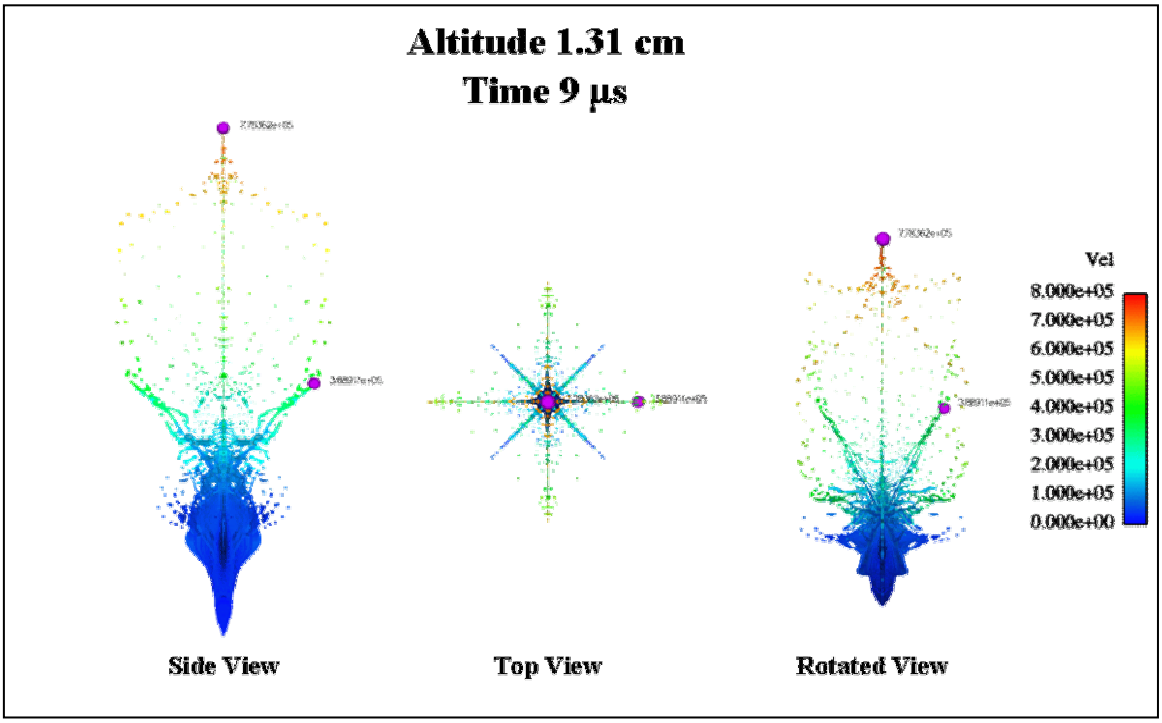

Figure 6. Formation of the 1.31-cm altitude pyramid charge at 9 µs.

Note that the probe near the tip region is not intended to capture the maximum jet particle velocity, just a region near the tip and not necessarily on the centerline of the charge. The collapse of the pyramidal liner illustrates a mechanism to control the distribution of the liner mass. The pyramid walls act as linear or cutting charges and interact with each other causing a spreading of the jet.

Figure 3 shows the same type of data for the pyramidal liner with an altitude of 0.7 cm at 11 µs. The tip velocity was 6.0 km/s, and the wing velocity has increased over the 0.5-cm case. Figure 4 shows the liner with 0.92-cm altitude at 10 µs. The tip velocity was 6.9 km/s, and the estimated wing velocity was about 4 km/s. Figure 5 increases the altitude to 1.0 cm, and at 10 µs the tip velocity is 7.1 km/s. The wing velocity is again about 4 km/s; recall that the positioning of the probe is somewhat arbitrary. Figure 6 shows the 1.31-cm altitude case at 9 µs with a tip velocity of 8.0 km/s and an approximate wing velocity of, again, ~4 km/s. Figure 7 plots the tip or maximum velocity as a function of time for each pyramid altitude up to the maximum run time for each case.

Recall that all jets were allowed to travel approximately the same distance, namely ~5 cm. The jet tip velocity increases as the altitude of the pyramid increases in approximately a linear fashion. Thus, the tip velocity increases as the pyramid apex angle (the angle between opposite faces) decreases, which is analogous to conventional shaped charges with conical liners where the jet tip velocity increases as the conical apex angle decreases. Also, by comparing the rotated views of Figures 2–6, the lateral spread of the jet decreases or the jet becomes more compact

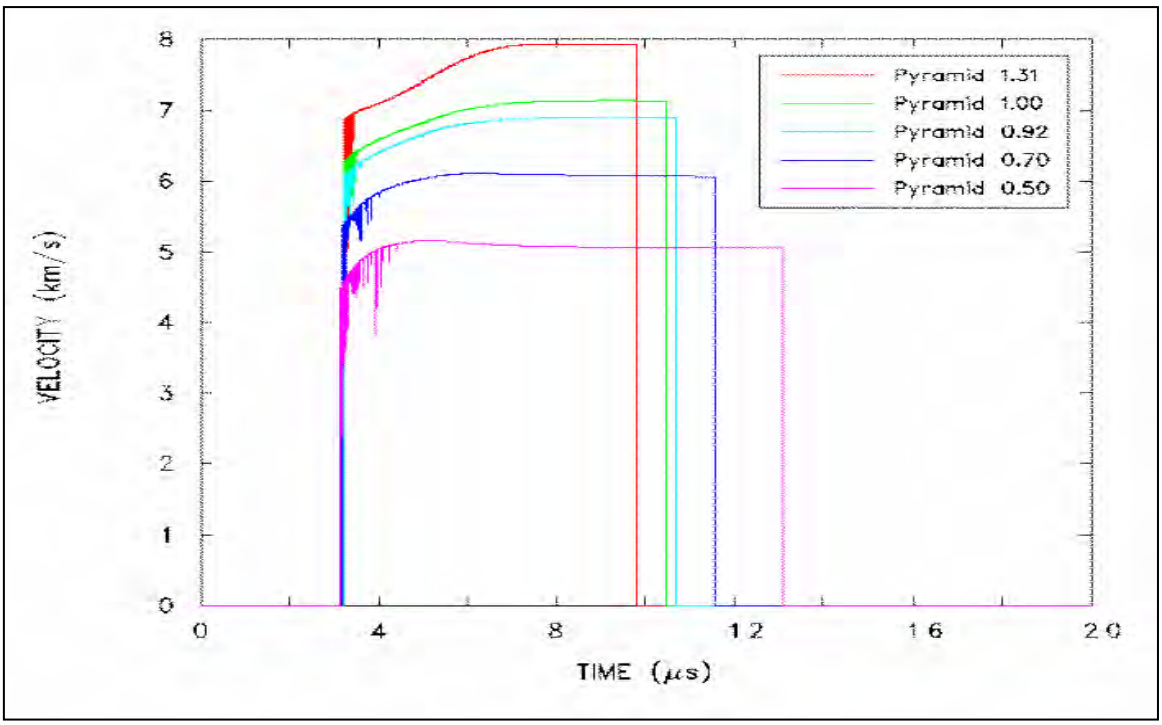

Figure 7. Jet tip velocity vs. time for various altitudes of the pyramidal charge.

as the altitude of the pyramidal liner decreases. Top views in these figures also illustrate this spread. Thus, increasing the apex or pyramid angle implies more compact projectiles (jets), which implies the jet material on the axis has more mass and hence a lower velocity. From the top and rotated views of Figures 2–6, the large, low velocity "blob" near the rear of jet increases as the altitude increases. This blob represents material that has not yet entered the jetting process, most of which will remain as the slug, analogous to conventional conical shaped charges. The numerical results previously presented conceptually agree with the flash x-rays obtained by Geiger and Honcia (1977); see also Walters and Zukas (1989). They reported a cross-shaped cut on target witness plates resulting from the interaction of the pyramidal faces with the cuts being parallel to the base sides of the pyramid. The numerical results presented in Figures 2–6 indicate a double cross, or jets with eight, not four, legs. However, as can be seen from top views in the figures from the color-coded legend, one of the crosses is traveling at a much lower velocity than the other (since it is part of the slug), which would result in minimal penetration into steel. Thus, the numerical simulations are in agreement with the origin of the cross-shaped cut reported by Geiger and Honcia (1977).

The next phase of the study involved picking the fastest jet from the previously mentioned study, namely the 1.31-cm altitude pyramid and changing the explosive geometry from a cylinder to a square with the same base area as the pyramidal liners and the same height as the explosive cylinder. The resulting explosive geometry is shown in Figure 8. The pyramid liner and charge characteristics are shown in Table 1, the only difference being the explosive charge mass which is 0.86799 g for the square explosive billet compared to 1.47877 g for the cylindrical billet. The

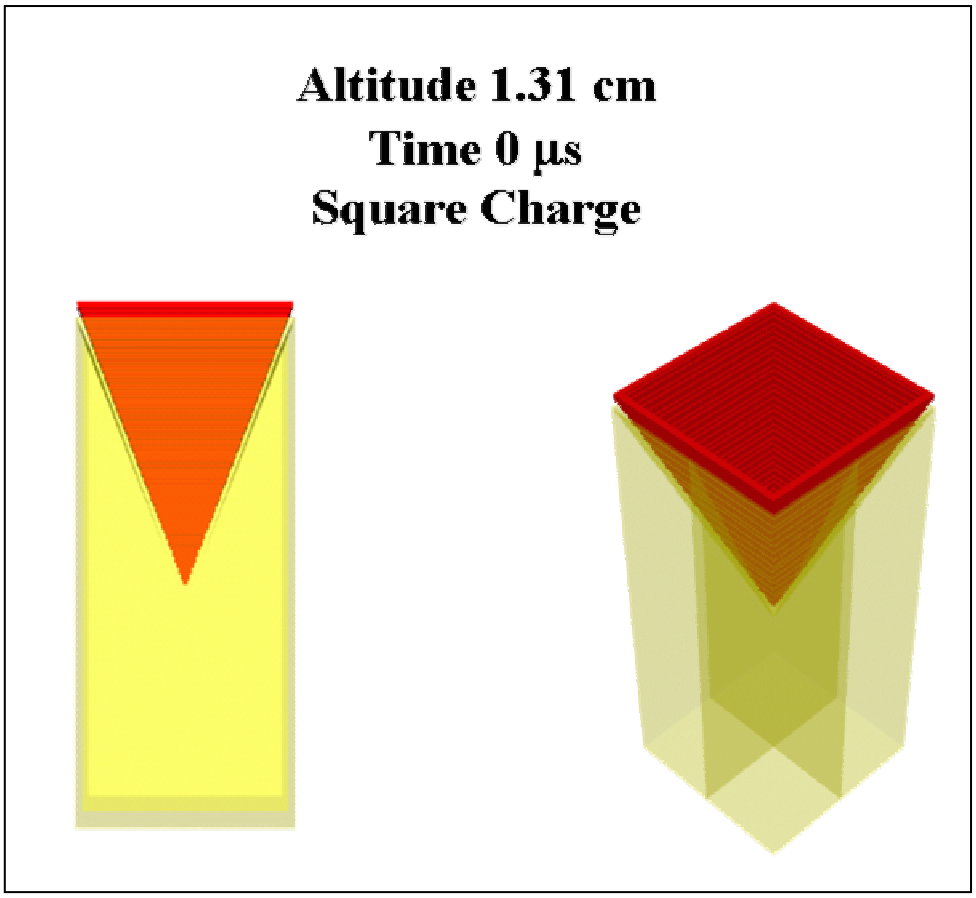

Figure 8. Initial geometry of the 1.31-cm altitude pyramidal liner with a square explosive billet.

first case allowed line wave detonation simultaneously around the four edges of the square base. The second case used four-point detonators at each corner of the base, and the third case used a five-point detonation, the fifth detonator being on the charge centerline. The fourth case was a simple single-point initiation used for direct comparison to the altitude study cases described earlier. These cases are shown in Figures 9–12 using the same format as Figures 2–6. Figure 9 shows the four-point initiation. This case generated the highest tip velocity of 9.7 km/s at 7 μs. Recall the point initiated 1.31-cm altitude case had a tip velocity of 8.0 km/s. The four-point initiation is analogous to a peripheral initiation of a standard shaped charge with a conical liner, which yields a higher tip velocity. This was also the most compact of the non-point initiated cases (recall from the previously mentioned cases, the jet becomes more compact as the velocity increases). Note also that the wing velocity is higher for four-point initiation as compared to the line wave or five-point case, based on the arbitrary position of the probe. Note that in these figures (top view), the second cross (from the slug) has not yet emerged and is moving at a very low velocity (i.e., only the fast wings have emerged). The second cross from the slug region emerged due to the larger amount of explosive around the base of the liner with the cylindrical charge (i.e., subcalibration of the liner, as can be seen by comparing Figures 1 and 8). Figure 10 shows the line wave detonation case at 8 μs with a tip velocity of 9.3 km/s. Figure 11 shows

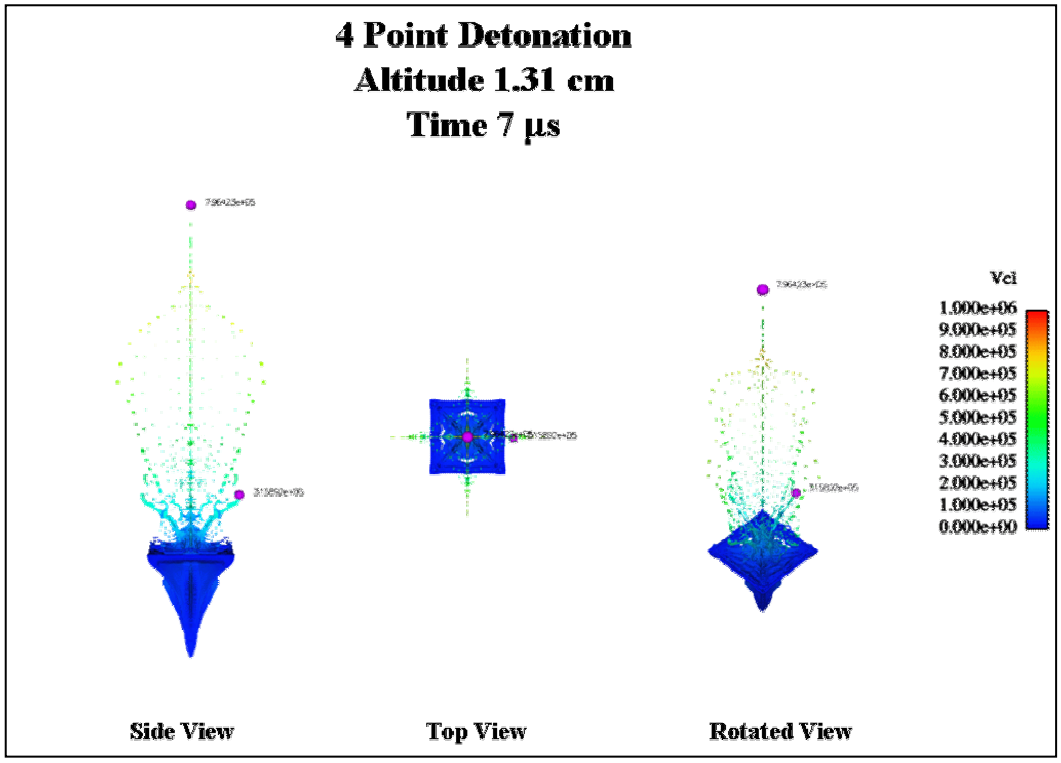

Figure 9. Formation of the 1.31-cm altitude pyramid charge at 7 µs using a square explosive billet and a four-point corner initiation.

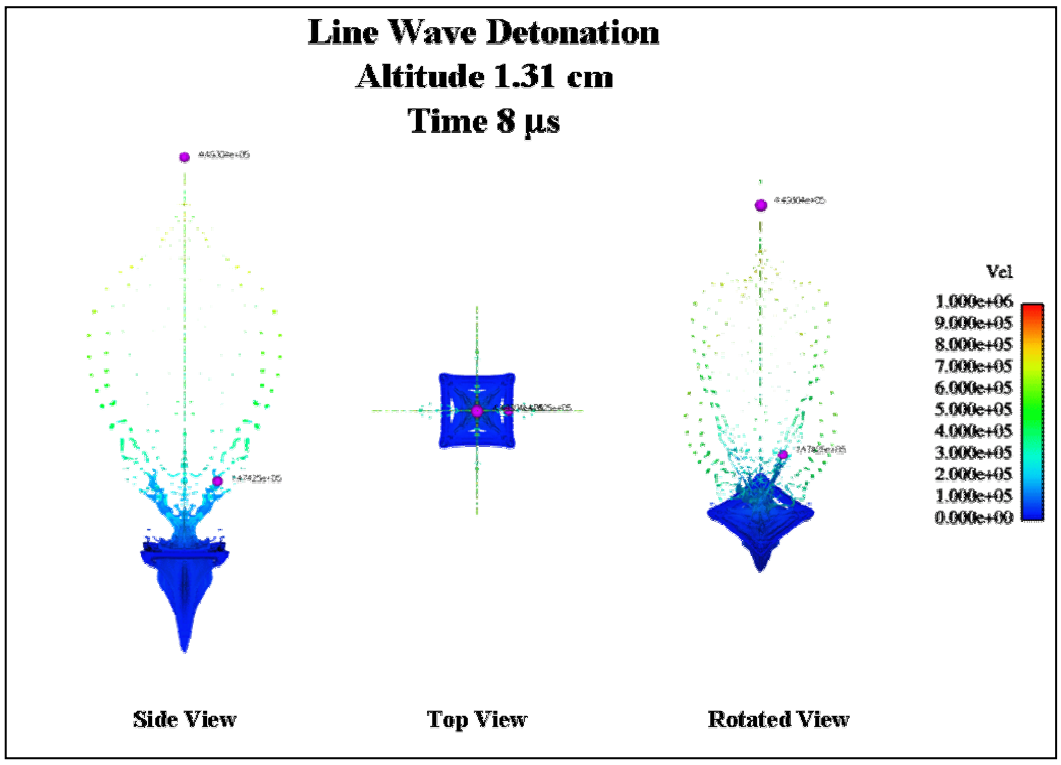

Figure 10. Formation of the 1.31-cm altitude pyramid charge at 8 µs using a square explosive billet and a line wave edge initiation.

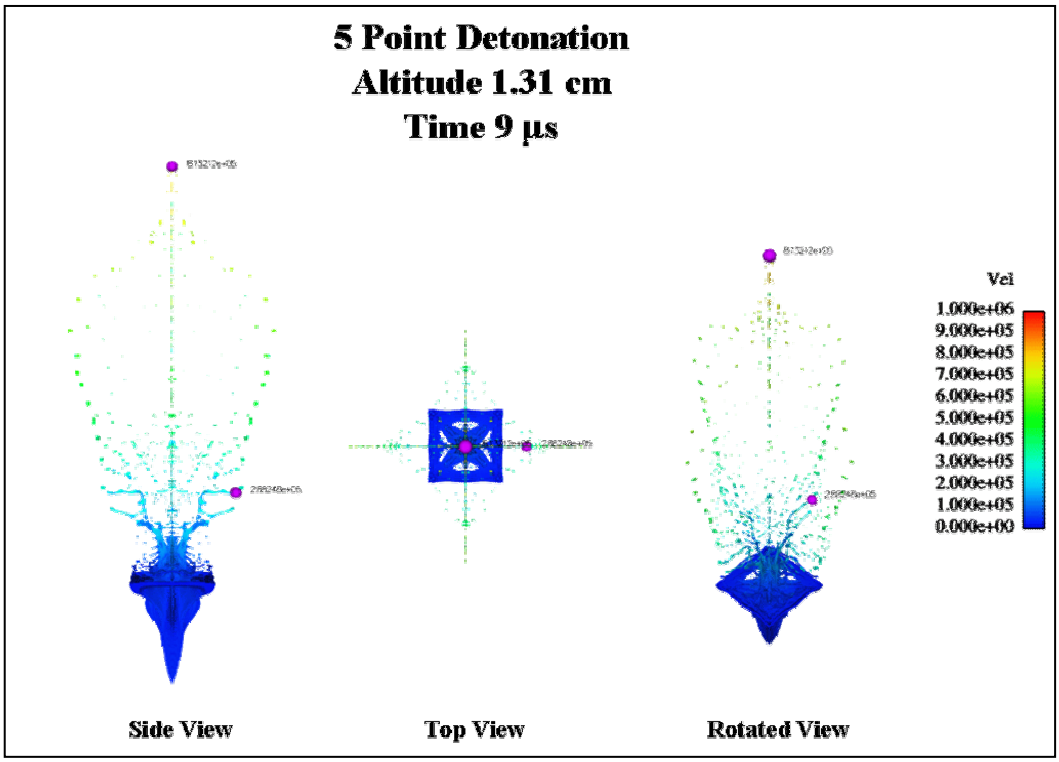

Figure 11. Formation of the 1.31-cm altitude pyramid charge at 9 µs using a square explosive billet and a five-point initiation.

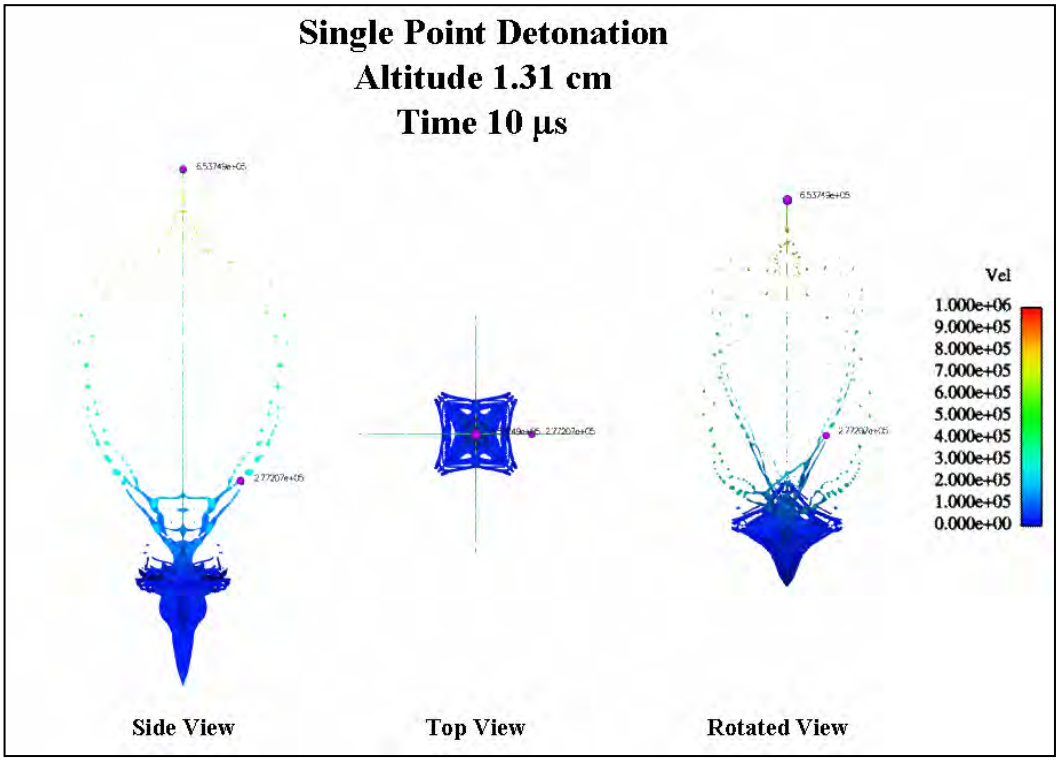

Figure 12. Formation of the 1.31-cm altitude pyramid charge at 10 µs using a square explosive billet and a single center-point initiation.

the five-point initiation at 9 μs with a tip velocity of 8.4 km/s and the case closest to Figure 6. It is likely that the centerline detonator, being closest to the liner apex, dominated the collapse, but a significant velocity increase (0.4 km/s) was observed. Figure 12 is a single center-point initiation case at 10 μs. The tip velocity dropped to 7.2 km/s. This velocity decrease probably results from the inefficient use of explosive since the detonation wave will generate a complex interaction with the corners of the charge. The rarefaction waves from the corner interactions probably influenced the pressure on the liner and hence the liner collapse velocity. However, the jet formation did not appear to be adversely affected. The four-point, five-point, and line wave detonation cases were analogous to a peripheral initiation case, which would minimize the influence of the corners of the square charge. Again, as with all the detonation mode cases, only the fast wings have emerged. Figure 13 plots velocity vs. time for the three detonation modes studied. The time in the plot of Figure 13 is the maximum time when the jet is still within the CTH mesh. Further studies regarding the explosive liner interaction for the square-based charges are recommended.

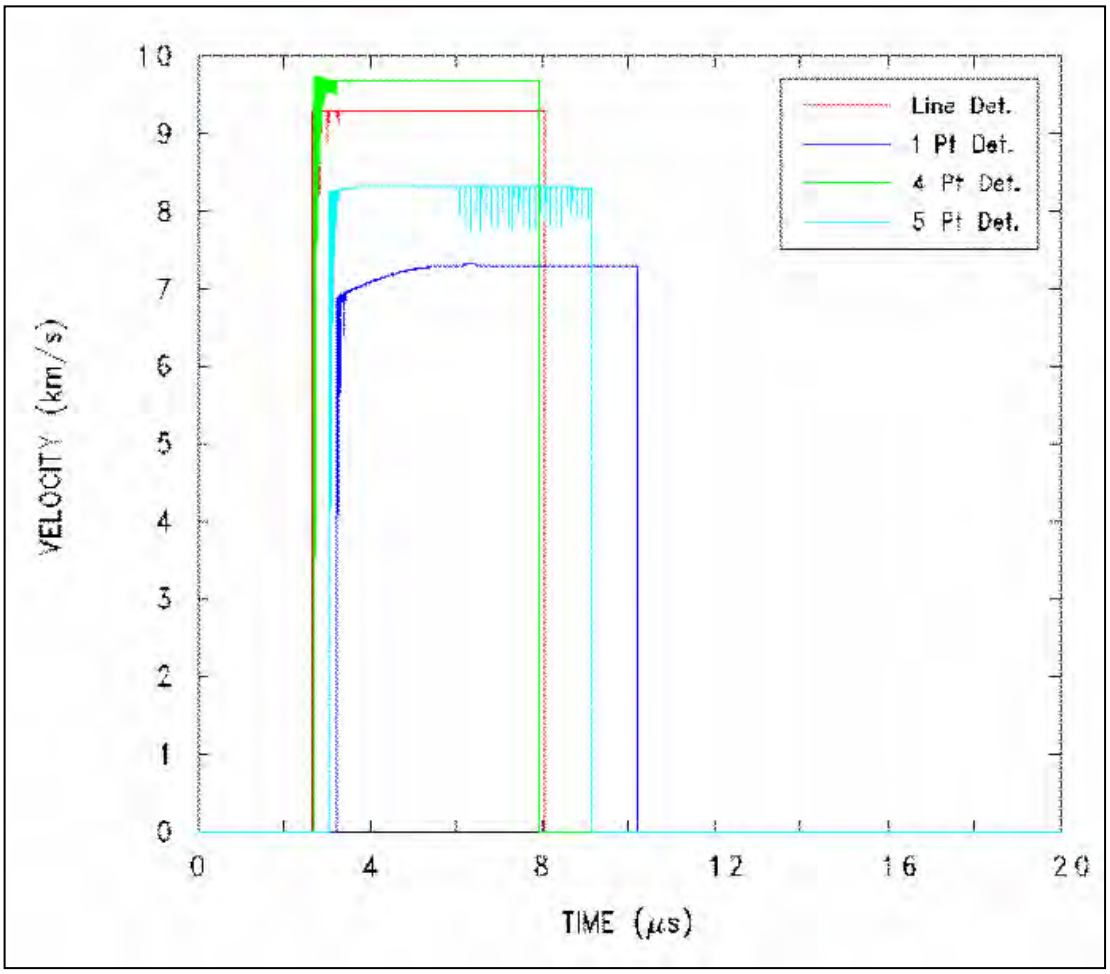

Figure 13. Jet tip velocity vs. time for various initiation modes using the square explosive billet.

4. Conclusion

This study is the first known set of numerical simulations of shaped charges with pyramidal liners and the first investigation of alternate modes of initiation for such charges. A shaped charge with a square base pyramidal liner is a device that can be used to distribute the projectile (jet) mass over a wider area at the expense of removing jet mass from the charge centerline. Devices of this nature may be effective against certain targets. The spread of the projectile can be controlled by varying the altitude or height or the pyramidal liner and altering the mode of initiation from a single symmetric point initiation. Also, the velocity of the projectile can be controlled by the liner altitude and initiation mode; in fact, the jet tip velocity ranged from 5.1 to 9.7 km/s in this study. The results presented herein are in conceptual agreement with the experimental study of Geiger and Honcia (1977) even though different base areas, different altitudes, different wall thicknesses, and even different explosive fills were used. The numerical simulations predicted a “double cross” pattern of the jet formation when the jet is viewed from the top. This double cross was not observed on the steel witness plates from the studies reported by Geiger and Honcia (1977) due to the fact that one “cross” is traveling at a relatively slow velocity compared to the other, since the slower cross is from the slug formation.

5. References

Bell, R. L.; Hertel Jr., E. S. *An Improved Material Interface Reconstruction Algorithm for Eulerian Codes;* SAND92-1716; Sandia National Laboratories: Albuquerque, NM, 1992.

Dobratz, B. M. *LLNL Explosives Handbook;* UCRL-5299; Lawrence Livermore Laboratory: Livermore, CA, 1981

Geiger, W.; Honcia, G. Shaped Charges With Pyramidal Liners. *Proceedings of the 3rd International Symposium on Ballistics,* Karlsruhe, Germany, 23–25 March 1977.

Johnson, G. R.; Cook, W. H. A Constitutive Model and Data Subjected to Large Strains, High Strain Rates and High Temperatures. *Proceedings of the 7th International Symposium on Ballistics,* The Hague, The Netherlands, 1983; p 541–548.

Johnson, G. R.; Cook, W. H. Fracture Characteristics of Three Metals Subjected to Various Strains, Strain Rates, Temperatures, and Pressures. *Journal of Engineering Fracture Mechanics* **1985**, *21* (1), 31–48.

Kerley, G. I. *CTH Equation of State Package: Porosity and Reactive Burn Models;* SAND92-0553, Sandia National Laboratories: Albuquerque, NM, 1992.

Lee, E. L.; Hornig, H. C.; Kury, J. W. *Adiabatic Expansion of High Explosive Detonation Products*; UCRL-50422; Lawrence Livermore National Laboratory: Livermore, CA, 1968.

McGlaun, J. M.; Thompson, S. L.; Elrick, M. G. CTH: A Three-Dimensional Shock Wave Physics Code. *International Journal of Impact Engineering* **1990,** *10* (1–4), 351–360.

Noh, W. F.; Woodward, P. SLIC (Simple Line Interface Calculation). *Lecture Notes in Physics;* Vol. 59; Springer-Verlag: New York, 1976.

Steinberg, D. J.; Lund, C. M. A Constitutive Model for Strain Rates From 10^{-4} to 10^{6} s^{-1}. *Journal of Applied Physics* **1989,** *65* (4), 1528–1533.

Steinberg, D. J.; Cochran, S. G.; Guinan, M. W. A Constitutive Model for Metals Applicable at High-Strain Rate. *Journal of Applied Physics* **1980**, *51* (3), 1498–1504.

Walters, W.; Zukas, J. *Fundamentals of Shaped Charges*; John Wiley & Sons: New York, 1989.

Zerilli, F. J.; Armstrong, R. W. Dislocation-Mechanics-Based Constitutive Relations for Material Dynamics Calculations. *Journal of Applied Physics* **1987,** *61* (5), 1816–1825.

INTENTIONALLY LEFT BLANK.

Appendix A. Input Deck for Pyramid Height Study

This appendix appears in its original form, without editorial change.

```
*

* id=1 - Starting baseline configuration
*
*eor*cgenin
*
Pyramid 0.50 cm height
*
control
  ep
  mmp
endcontrol
*
mesh
  block  geometry 3dr  type e
    x0=0.0
      x1  n=130  dxf=0.01 rat=1.
    endx
    y0=-2.5
      y1  n=750  dyf=0.01 rat=1.
    endy
    z0=0.0
      z1  n=130  dzf=0.01 rat=1.
    endz
*    xact=0.0,1.0
*    yact=0.0,5.0
  endblock
endmesh
*
insertion of material
  block 1
*
* NOTE: From of steel cover sit at x-coordinate origin.
*
    package 'Copper Pyramid'
      material 1
      numsub 10
      insert pyramid
        p1      0.4950   0.0000   0.0000
        p2      0.4950   0.0000   0.4950
        p3      0.0000   0.0000   0.4950
        p4      0.0000   0.0000   0.0000
*
* NOTE: Uncomment line to select pyramid height.
*       Currently 0.50 cm Pyramid is the selected height.
*
```

```
      ve     0.0000  -0.5000   0.0000
*       ve     0.0000  -0.7000   0.0000
*       ve     0.0000  -0.9200   0.0000
*       ve     0.0000  -1.0000   0.0000
*       ve     0.0000  -1.3100   0.0000
    endinsert
*
* NOTE: Below is for 0.50 cm height pyramid
*
    delete pyramid
      p1     0.4105   0.0000   0.0000
      p2     0.4105   0.0000   0.4105
      p3     0.0000   0.0000   0.4105
      p4     0.0000   0.0000   0.0000
      ve     0.0000  -0.4105   0.0000
    enddelete
*
* NOTE: Uncomment below for 0.70 cm height pyramid
*
*     delete pyramid
*       p1     0.4215   0.0000   0.0000
*       p2     0.4215   0.0000   0.4215
*       p3     0.0000   0.0000   0.4215
*       p4     0.0000   0.0000   0.0000
*       ve     0.0000  -0.5961   0.0000
*     enddelete
*
* NOTE: Uncomment below for 0.92 cm height pyramid
*
*     delete pyramid
*       p1     0.4268   0.0000   0.0000
*       p2     0.4268   0.0000   0.4268
*       p3     0.0000   0.0000   0.4268
*       p4     0.0000   0.0000   0.0000
*       ve     0.0000  -0.7934   0.0000
*     enddelete
*
* NOTE: Uncomment below for 1.00 cm height pyramid
*
*     delete pyramid
*       p1     0.4280   0.0000   0.0000
*       p2     0.4280   0.0000   0.4280
*       p3     0.0000   0.0000   0.4280
*       p4     0.0000   0.0000   0.0000
*       ve     0.0000  -0.8647   0.0000
*     enddelete
```

```
*
* NOTE: Uncomment below for 1.31 cm height pyramid
*
*     delete pyramid
*       p1      0.4308   0.0000   0.0000
*       p2      0.4308   0.0000   0.4308
*       p3      0.0000   0.0000   0.4308
*       p4      0.0000   0.0000   0.0000
*       ve      0.0000  -1.1402   0.0000
*     enddelete
   endpackage
*
   package 'HMX Explosive'
     material 2
     numsub 10
     insert cylinder
       ce1     0.0000   0.0000   0.0000
       ce2     0.0000  -2.3100   0.0000
       radius 0.7
     endi
     delete pyramid
       p1      0.4950   0.0000   0.0000
       p2      0.4950   0.0000   0.4950
       p3      0.0000   0.0000   0.4950
       p4      0.0000   0.0000   0.0000
*
* NOTE: Uncomment line to select pyramid height.
*       Currently 0.50 cm Pyramid is the selected height.
*
       ve      0.0000  -0.5000   0.0000
*       ve      0.0000  -0.7000   0.0000
*       ve      0.0000  -0.9200   0.0000
*       ve      0.0000  -1.0000   0.0000
*       ve      0.0000  -1.3100   0.0000
     enddelete
   endpackage
*
  endblock
endinsertion
*
epdata
*
  matep 1  johnson-cook copper poisson 0.34
  vpsave
  mix 3
endep
```

```
*
eos
  mat1 mgrun  copper
  mat2 jwl    hmx
endeos
*
heburn
  material 2  d 9.11e5  pre 1.0e12
    dp 0.000 -2.3099 0.000 ti 0.0  radius 0.05
endheburn
*
tracer
  add  0.0  -0.02    0.0
endtracer
*
*eor*cthin
*
Pyramid 0.50 cm height
*
control
  tstop=20.e-6
  cpshift=900.
  rdumpf=3600
  ntbad 100000000
endcontrol
*
*restart
*  time=3.0e-6
*endr
*
cellthermo
  mmp2
endcell
*
convct
  convect=1
  interface=high
endc
*
discard
*  material 1  density  -.001 pressure 1.0e12  ton 1.1e-6
  material 2  density -0.01  pressure 5.0e6   ton 2.0e-6 toff 4.0e-6
  material 2  density 10.00  pressure 1.0e12  ton 3.0e-6 toff 4.1e-6
endd
*
edit
```

```
  shortt
    time=0.  dtf=10000.
  ends
  longt
    time=0.  dtf=10000.
  endl
  plott
    time=0.  dtf=0.05e-6
  endp
  plotdata
    volume
    mass
    temperature
    pressure
    velocity
  endplotdata
  restt
    time=0   dtf=1.e-6
  endr
  histc
    cycle=0  dcfreq=1
      htracer1
  endh
endedit
*
mindt
  time=0.  dtmin=1.0e-13
endm
*
fracts
  pressure
  pfrac1=-3.45e9
  pfrac2= -1e9
  pfmix =-5.0E20
  pfvoid=-5.0E20
endf
*
boundary
  bhydro
    block=1
      bxbot 0
      bxtop 1
      bybot 1
      bytop 1
      bzbot 0
      bztop 1
```

```
    endb
  endh
endb
*
*eor*pltin
*
```

INTENTIONALLY LEFT BLANK.

Appendix B. Input Deck for Detonation Location Study

This appendix appears in its original form, without editorial change.

```
*
* id=1 - Starting baseline configuration
*
*eor*cgenin
*
Pyramid 1.31 cm height 1 point detonation
*
control
  ep
  mmp
endcontrol
*
mesh
  block  geometry 3dr  type e
    x0=0.0
      x1  n=130  dxf=0.01 rat=1.
    endx
    y0=-2.5
      y1  n=750  dyf=0.01 rat=1.
    endy
    z0=0.0
      z1  n=130  dzf=0.01 rat=1.
    endz
*    xact=0.0,1.0
*    yact=0.0,5.0
  endblock
endmesh
*
insertion of material
  block 1
*
* NOTE: From of steel cover sit at x-coordinate origin.
*
    package 'Copper Pyramid'
      material 1
      numsub 10
      insert pyramid
        p1      0.4950   0.0000   0.0000
        p2      0.4950   0.0000   0.4950
        p3      0.0000   0.0000   0.4950
        p4      0.0000   0.0000   0.0000
        ve      0.0000  -1.3100   0.0000
      endinsert
      delete pyramid
        p1      0.4308   0.0000   0.0000
        p2      0.4308   0.0000   0.4308
```

```
      p3      0.0000   0.0000   0.4308
      p4      0.0000   0.0000   0.0000
      ve      0.0000  -1.1402   0.0000
    enddelete
  endpackage
*
  package 'HMX Explosive'
    material 2
    numsub 10
    insert box
      p1      0.0000   0.0000   0.0000
      p2      0.4950  -2.3100   0.4950
    endi
    delete pyramid
      p1      0.4950   0.0000   0.0000
      p2      0.4950   0.0000   0.4950
      p3      0.0000   0.0000   0.4950
      p4      0.0000   0.0000   0.0000
      ve      0.0000  -1.3100   0.0000
    enddelete
  endpackage
*
 endblock
endinsertion
*
epdata
*
 matep 1  johnson-cook copper poisson 0.34
 vpsave
 mix 3
endep
*
eos
 mat1 mgrun  copper
 mat2 jwl    hmx
endeos
*
heburn
 material 2  d 9.11e5  pre 1.0e12
*
* NOTE: Uncomment appropriate line for selected initiation type.
*
* NOTE: 1 Point initiation. Currently selected.
*
   dp 0.000 -2.3099 0.000 ti 0.0  radius 0.05
*
```

```
* NOTE: 4 Point initiation. Currently not selected.
*
*    dp 0.495 -2.3099 0.495 ti 0.0  radius 0.05
*
* NOTE: 5 Point initiation. Currently not selected.
*
*    dp 0.495 -2.3099 0.495 ti 0.0  radius 0.05
*    dp 0.000 -2.3099 0.000 ti 0.0  radius 0.05
*
* NOTE: Peripheral Line initiation. Currently not selected.
*
*    dl 0.495 -2.3099 0.000 to 0.495 -2.3099 0.495 ti 0.0  radius 0.05
*    dl 0.000 -2.3099 0.495 to 0.495 -2.3099 0.495 ti 0.0  radius 0.05
endheburn
*
tracer
  add  0.0  -0.02    0.0
endtracer
*
*eor*cthin
*
Pyramid 1.31 cm height 1 point detonation
*
control
  tstop=20.e-6
  cpshift=900.
  rdumpf=3600
  ntbad 100000000
endcontrol
*
*restart
*  time=3.0e-6
*endr
*
cellthermo
  mmp2
endcell
*
convct
  convect=1
  interface=high
endc
*
discard
*  material 1  density  -.001 pressure 1.0e12  ton 1.1e-6
  material 2  density -0.01  pressure 5.0e6   ton 2.0e-6 toff 4.0e-6
```

```
  material 2  density 10.00  pressure 1.0e12  ton 3.0e-6 toff 4.1e-6
endd
*
edit
  shortt
    time=0.  dtf=10000.
  ends
  longt
    time=0.  dtf=10000.
  endl
  plott
    time=0.  dtf=0.05e-6
  endp
  plotdata
    volume
    mass
    temperature
    pressure
    velocity
  endplotdata
  restt
    time=0   dtf=1.e-6
  endr
  histc
    cycle=0  dcfreq=1
      htracer1
  endh
endedit
*
mindt
  time=0.  dtmin=1.0e-13
endm
*
fracts
  pressure
  pfrac1=-3.45e9
  pfrac2= -1e9
  pfmix =-5.0E20
  pfvoid=-5.0E20
endf
*
boundary
  bhydro
    block=1
      bxbot 0
      bxtop 1
```

```
      bybot 1
      bytop 1
      bzbot 0
      bztop 1
    endb
  endh
endb
*
*eor*pltin
*
```

NO. OF COPIES	ORGANIZATION
2	DEFENSE TECHNICAL INFORMATION CENTER DTIC OCA 8725 JOHN J KINGMAN RD STE 0944 FT BELVOIR VA 22060-6218
1	COMMANDING GENERAL US ARMY MATERIEL CMD AMCRDA TF 5001 EISENHOWER AVE ALEXANDRIA VA 22333-0001
1	INST FOR ADVNCD TCHNLGY THE UNIV OF TEXAS AT AUSTIN 3925 W BRAKER LN STE 400 AUSTIN TX 78759-5316
1	US MILITARY ACADEMY MATH SCI CTR EXCELLENCE MADN MATH THAYER HALL WEST POINT NY 10996-1786
1	DIRECTOR US ARMY RESEARCH LAB AMSRL D DR D SMITH 2800 POWDER MILL RD ADELPHI MD 20783-1197
1	DIRECTOR US ARMY RESEARCH LAB AMSRL CS IS R 2800 POWDER MILL RD ADELPHI MD 20783-1197
3	DIRECTOR US ARMY RESEARCH LAB AMSRL CI OK TL 2800 POWDER MILL RD ADELPHI MD 20783-1197
3	DIRECTOR US ARMY RESEARCH LAB AMSRL CS IS T 2800 POWDER MILL RD ADELPHI MD 20783-1197

NO. OF COPIES	ORGANIZATION
	ABERDEEN PROVING GROUND
2	DIR USARL AMSRL CI LP (BLDG 305) AMSRL CI OK TP (BLDG 4600)

NO. OF COPIES	ORGANIZATION
3	COMMANDER US ARMY ARDEC AMSTA AR WEE C E BAKER A DANIELS R FONG B3022 PICATINNY ARSENAL NJ 07806-5000
2	COMMANDER US ARMY AVN & MISSILE CMD AMSAM RD PS WF S HILL S HOWARD REDSTONE ARSENAL AL 35898-5247
3	COMMANDER US ARMY RESEARCH OFFFICE S F DAVIS K IYER A RAJENDRAN PO BOX 12211 RTP NC 27709-2211
1	COMMANDER NAVAL WEAPONS CTR N FASIG CODE 3261 CHINA LAKE CA 93555
1	COMMANDER NVL SURFACE WARFARE CTR DAHLGREN DIVISION W E HOYE G22 17320 DAHLGREN RD DAHLGREN VA 22448-5100
5	COMMANDER NAVL SURFACE WARFARE CTR DAHLGREN DIVISION R GARRETT G22 W E HOYE G22 T SPIVAK G22 P WALTER F ZERILLI 17320 DAHLGREN RD DAHLGREN VA 22448-5100

NO. OF COPIES	ORGANIZATION
2	AIR FORCE ARMAMENT LAB AFATL DLJR J FOSTER D LAMBERT EGLIN AFB FL 32542-6810
2	DARPA W SNOWDEN S WAX 3701 N FAIRFAX DR ARLINGTON VA 22203-1714
2	LOS ALAMOS NATL LAB P HOWE MS P915 J KENNEDY MS P915 PO BOX 1663 LOS ALAMOS NM 87545
2	LOS ALAMOS NATL LAB L HULL MS A133 J V REPA MS A133 PO BOX 1663 LOS ALAMOS NM 87545
3	SANDIA NATL LAB MAIL SERVICES MS 0100 M FORRESTAL DIV 1551 E HERTEL M VIGIL MS 0819 PO BOX 5800 ALBUQUERQUE NM 87185-0100
3	DIR LLNL D BAUM L099 M MURPHY C SIMONSON MS PO BOX 808 MS L35 LIVERMORE CA 94550
2	SOUTHWEST RESEARCH INST C ANDERSON J WALKER PO DRAWER 28510 SAN ANTONIO TX 78228-0510
2	AEROJET J CARLEONE S KEY PO BOX 13222 SACRAMENTO CA 95813-6000

NO. OF COPIES	ORGANIZATION
1	ALLIANT TECHSYSTEMS INC R TOMPKINS 5050 LINCOLN DR EDINA MN 55436
1	CMPTNL MECHS CNSLTNTS J A ZUKAS PO BOX 11314 BALTIMORE MD 21239-0314
3	DETK R CICCARELLI W FLIS M MAJERUS 3620 HORIZON DR KING OF PRUSSIA PA 19406
1	RAYTHEON MSL SYS CO T STURGEON BLDG 805 MS D4 PO BOX 11337 TUCSON AZ 85734-1337
1	TEXTRON DEFENSE SYSTEMS C MILLER 201 LOWELL ST WILMINGTON MA 01887-4113
1	D R KENNEDY & ASSOC INC D KENNEDY PO BOX 4003 MOUNTAIN VIEW CA 94040
1	LOCKHEED MARTIN ELECTRONICS & MISSILES G W BROOKS 5600 SAND LAKE RD MP 544 ORLANDO FL 32819-8907
4	GD OTS C ENGLISH T GRAHAM D A MATUSKA J OSBORN 4565 COMMERCIAL DR A NICEVILLE FL 32578
2	GD OTS D BOEKA N OUYE 400 ESTUDILLO AVE STE 100 SAN LEANDRO CA 94577-0205
1	ZERNOW TECHNICAL SVS INC L ZERNOW 425 W BONITA AVE STE 208 SAN DIMAS CA 91773
1	PM JAVELIN PO SSAE FS AM EG C ALLEN REDSTONE ARSENAL AL 35898-5720
1	PM TOW SFAE TS TO J BIER REDSTONE ARSENAL AL 35898-5720
1	HALLIBURTON ENERGY SVCS JET RESEARCH CENTER D LEIDEL PO BOX 327 ALVARADO TX 76009-9775
1	J VAROSH PO BOX 359 TRACY CA 95378
1	DIR LLNL R VAROSH L149 PO BOX 808 LIVERMORE CA 90550
3	INST FOR ADVNCD TECH S BLESS H FAN W REINECKE 3925 W BRAKER LN STE 400 AUSTIN TX 78759-5316
1	NORTHROP GRUMMAN DR D PILLASCH B57 D3700 PO BOX 296 1100 W HOLLYVALE ST AZUSA CA 91702
1	INTRNTL RSRCH ASSOC D ORPHAL 4450 BLACK AVE PLEASANTON CA 94566-6105

NO. OF
COPIES ORGANIZATION

ABERDEEN PROVING GROUND

45 DIR USARL
AMSRL WM
B BURNS
E SCHMIDT
J SMITH
AMSRL WM MD
W DEROSSET
R DOWDING
AMSRL WM T
T HAVEL
M ZOLTOSKI
AMSRL WM TA
W BRUCHEY
M BURKINS
W GILLICH
W GOOCH
M KEELE
J RUNYEON
AMSRL WM TB
P BAKER
R LOTTERO
J STARKENBERG
AMSRL WM TC
T W BJERKE
G BOYCE
R COATES
T FARRAND
E KENNEDY
K KIMSEY
L MAGNESS
D SCHEFFLER (6 CPS)
S SCHRAML
B SORENSEN
R SUMMERS
W WALTERS (10 CPS)
AMSRL WM TD
K FRANK
E RAPACKI
S SEGLETES